Available online at www.sciencedirect.com
SCIENCE DIRECT®
Physica C 412–414 (2004) 1376–1382
PHYSICA C
www.elsevier.com/locate/physc

Electron microscopy of MgB_2 thin film on YSZ-buffered Hastelloy

Harini Sosiati [a,b,*], S. Hata [c], N. Kuwano [b], Y. Tomokiyo [c], A. Matsumoto [d], M. Fukutomi [d], H. Kitaguchi [d], K. Komori [d], H. Kumakura [d]

[a] *Research Laboratory for High Voltage Electron Microscopy, Kyushu University, Fukuoka 812-8581, Japan*
[b] *Art, Science and Technology Center for Cooperative Research, Kyushu University, 6-1 Kasuga Kouen, Fukuoka 816-8580, Japan*
[c] *Department of Applied Science for Electronics and Materials, Kyushu University, Fukuoka 816-8580, Japan*
[d] *National Institute for Materials Science, Tsukuba 305-0047, Japan*

Received 29 October 2003; accepted 13 January 2004
Available online 11 June 2004

Abstract

In order to understand the relationship between the microstructures and superconducting properties of MgB_2 films, analytical TEM observations have been carried out. The films were fabricated by a KrF excimer laser deposition on Hastelloy substrates precoated with YSZ (yttria-stabilized zirconia). The deposited films were annealed under Ar atmosphere at 873 K for 1 h and at 953 K for 0.5 h. The critical current densities of these films were measured to be $J_c = 1 \times 10^5$ A/cm^2 and $J_c = 7.7 \times 10^3$ A/cm^2 at 4.2 K and 10 T, respectively. The conventional TEM observation showed nanocrystalline MgB_2 and MgO of 5–30 nm in size dispersed in the films. Voids with various sizes from 10 to 60 nm were also observed in the films. Two-dimensional elemental analyses exhibited that near the MgB_2/YSZ interface the films have a layered structure where the layers enriched with Mg and O have low B concentrations complementarily. The average sizes of the MgB_2 and MgO grains and the voids increase with the annealing temperature. The enhancement of J_c value of the film annealed at 873 K may be due to smaller sizes of the MgB_2 and MgO grains and voids than those at 953 K.

PACS: 74.76.–w; 74.62.Bf; 74.60.Jg
Keywords: MgB_2; Thin film; Transmission electron microscopy

1. Introduction

Since the discovery of a new MgB_2 superconductor in 2001 [1], great interest in both fundamental studies and practical applications of the MgB_2 has strongly increased. Compared with conventional metallic superconductors such as Nb–Ti and Nb_3Sn, the MgB_2 has some advantages. The superconductivity of MgB_2 can be applied

* Corresponding author. Present address: Art, Science and Technology Center for Cooperative Research, Kyushu University, 6-1 Kasuga Kouen, Kasuga-shi, Fukuoka 816-8580, Japan. Tel.: +81-92-583-7885; fax: +81-92-573-8729.
E-mail address: harini@astec.kyushu-u.ac.jp (H. Sosiati).

0921-4534/$ - see front matter © 2004 Elsevier B.V. All rights reserved.
doi:10.1016/j.physc.2004.01.168

at higher temperature (20–30 K) region due to its higher transition temperature, and the material can be fabricated relatively easily in the form of tape, wire and thin film. These attractive properties make MgB_2 a good candidate for materials used in superconducting electronic devices.

Komori et al. [2] reported that MgB_2 thin films deposited on YSZ (yttria-stabilized zirconia)-buffered Hastelloy substrates show a good potential under magnetic field; i.e. the critical temperature T_c of about 30 K and J_c of 1×10^5 A/cm^2 at 4.2 K and 10 T. It has been indicated that nanocrystalline grains of MgB_2 less than 10 nm in size and of MgO around 10 nm are observed in the thin film. In a high magnetic field, the value of J_c is higher than that of thin films deposited on other substrates, as summarized in Ref. [3]. The relationship between the microstructure and J_c however, has not been clarified.

Most investigations of MgB_2-based materials focused on how to improve the superconducting properties such as the critical current density, J_c by varying methods of fabrication. The heat treatment condition is one of the most significant fabrication factors which give an impact on the superconducting property. It has been reported that with increasing the heat treatment temperature, the density of the film decreases, the porosity of MgB_2 increases and J_c then decreases [4].

In the present study, an analytical TEM (transmission electron microscopy) study of the MgB_2 thin films deposited on the YSZ-buffered Hastelloy substrates with different J_c and T_c values have been carried out. The aims of the present study are (1) to characterize the microstructure of the films in order to clarify the existence of nanocrystalline MgB_2 and MgO and (2) to analyze the distribution of magnesium, boron and oxygen. The effect of the microstructures on J_c and T_c values will be discussed. The present result will give some useful information for improving the product quality and understanding the mechanism of the superconductivity in the MgB_2 thin film.

2. Experimental

MgB_2 thin films about 0.5 μm in thickness were deposited on the Hastelloy (C-276) substrates which were precoated with 0.5–1 μm of YSZ as a buffer layer. MgB_2 thin films were fabricated by a pulsed laser deposition (PLD) method. A KrF excimer laser with 400 mJ/pulse operated at 5 Hz was used for the deposition. The cross-section of the MgB_2 film specimen is schematically shown in Fig. 1. The deposition of the MgB_2 thin film was conducted on the unheated YSZ/Hastelloy substrates in a 6×10^{-5} Torr Ar atmosphere for 40 min. A magnesium-enriched MgB_2 target for the PLD was prepared by mixing MgB_2 powder (Alfa Aesar) and magnesium powder (purity 99.9%) and pressing into a pellet. The ratio of Mg to B was set to be 2:1 molar ratio. The deposited films were then annealed in Ar atmosphere at 873 K for 1 h (specimen A) and at 953 K for 0.5 h (specimen B). The description of the investigated specimens is summarized in Table 1.

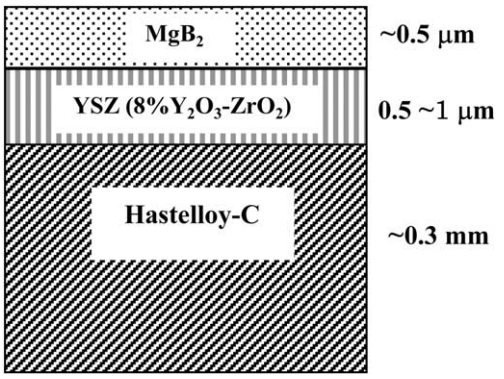

Fig. 1. Schematic cross-section of MgB_2 thin film specimen.

Table 1
Description of investigated specimens

Specimen	Annealing temperature (K)	Annealing time (h)	J_c at 10 T (A/cm^2)	T_c (K)
A	873	1	1×10^5	30
B	953	0.5	7.7×10^3	32

Cross-sectional TEM specimens were prepared by a focused ion beam (FIB)-microsampling technique with a Ga^+ ion source operated at 30 kV. TEM observation was carried out with microscopes of TECNAI 20 (FEI), TECNAI 20F (FEI) and JEM-2010FEF (JEOL) operated at 200 kV. In the present study, the EELS (electron energy loss spectroscopy) and STEM-EDS (scanning TEM energy dispersive X-ray spectroscopy) techniques were used for two-dimensional analyses for magnesium, boron and oxygen. The three-window technique was adopted in the EELS mapping. The boron-K edge at 188 eV, the oxygen-K edge at 532 eV and the magnesium-L edge at 55 eV was selected for the elemental mapping. The electron probe size in the STEM-EDS analysis with TECNAI 20F was about 1 nm in diameter.

3. Experimental results

3.1. Microstructure observations

Fig. 2(a) shows typical cross-sectional bright field TEM image of specimen A. The deposited MgB_2 layer exhibits fine dark spots about 5–20 nm in size, distributed homogeneously in the matrix. An under-focused image in Fig. 2(b) clearly shows the presence of voids whose size range is from 10 to 50 nm. Some large voids as indicated by arrows were made from the enlargement of the small voids due to electron radiation during the STEM-EDS analysis.

The electron diffraction shows a ring pattern, as in Fig. 2(c), suggesting that the film is made of fine crystalline domains. Indexing the ring pattern revealed that the domains are of MgB_2 and MgO.

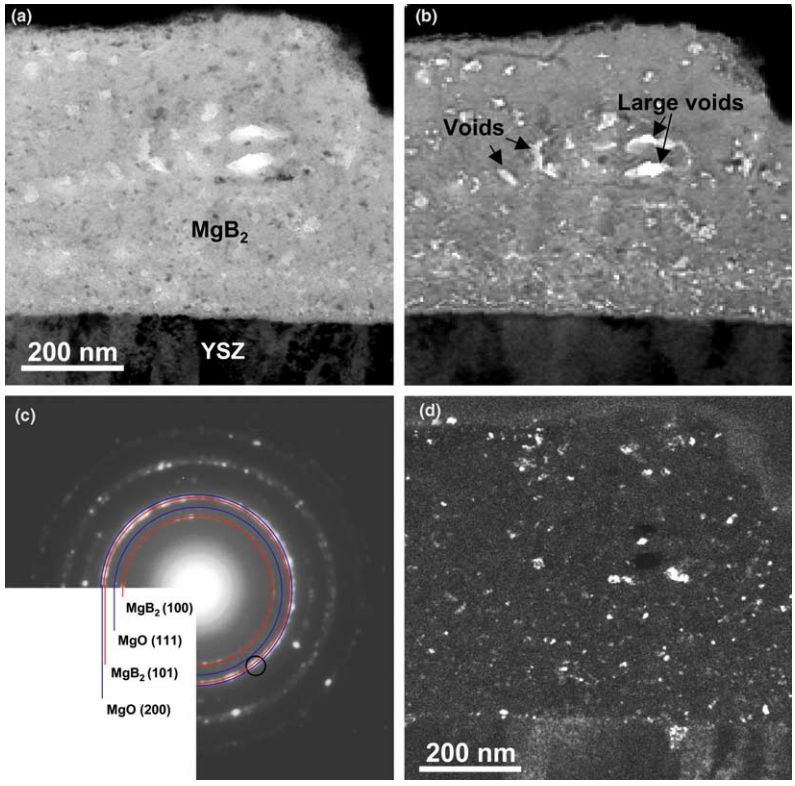

Fig. 2. Cross-sectional TEM image of specimen A: (a) bright field image, (b) under-focused BFI, (c) electron diffraction pattern obtained from the MgB_2 film and (d) dark field image taken with a part of the diffraction ring shown by a small circle in (c).

No other phases, such as MgB_4 and MgB_7 were detected. The dark field image taken with the 1 0 1MgB_2 and 2 0 0MgO reflections (Fig. 2(d)) clearly shows that a number of fine domains are distributed homogeneously, corresponding to the fine dark spots in Fig. 2(a). The size distribution of the nanocrystalline MgB_2 and MgO was characterized to be from 5 nm to 20 nm. It is difficult to distinguish clearly between the MgB_2 and MgO phases from the dark field imaging because the diffraction rings for the MgB_2 and MgO phases lay very close to each other; e.g. 1 0 1MgB_2 and 2 0 0MgO.

Fig. 3 shows a typical HRTEM (high resolution transmission electron microscopy) image. The lattice fringes indicate the existence of nanocrystalline MgB_2 or MgO phases. It can be seen that the MgB_2 or MgO grains are in contact well with each other, as drawn by white lines in Fig. 3. Most regions without the lattice fringes are explained to be the MgB_2 or MgO phases that do not satisfy the Bragg conditions, since the electron diffraction pattern in Fig. 2(c) shows no clear hollow intensity profiles suggesting the existence of amorphous phases.

3.2. Elemental mapping

Fig. 4 demonstrates a typical result of the EELS mapping for specimen A. One can see that in the middle-upper part of the MgB_2 film, some small areas where magnesium and oxygen are enriched have low boron concentration. The small areas may be the MgO phase. Interestingly, a magnesium- and oxygen-rich layer is present close to the MgB_2/YSZ interface and a boron-rich layer is sandwiched between the first and second magnesium- and oxygen-rich layers (regions labeled I and II in Fig. 4(b) and (d)). These appear as ''the layered structure''. In addition, the STEM-EDS mapping showed a good qualitative agreement with the ELLS mapping described above.

3.3. Effect of annealing temperature on microstructure

The increase of the annealing temperature to 953 K changes the microstructural features of specimen B, as shown in Fig. 5. The average grain size of MgB_2 and MgO slightly increases to the size from 5 to 30 nm, as clearly seen in Fig. 5(d). An under-focused image in Fig. 5(b) shows that the average size of voids also increases to the size from 10 to 60 nm. The center part of the electron diffraction pattern in Fig. 5(c) is diffuse, suggesting the presence of amorphous phase. These structural features may reduce the densification and grain connectivity of MgB_2 in specimen B. It was found from the EELS and STEM-EDS analyses that there are no clear differences in the elemental

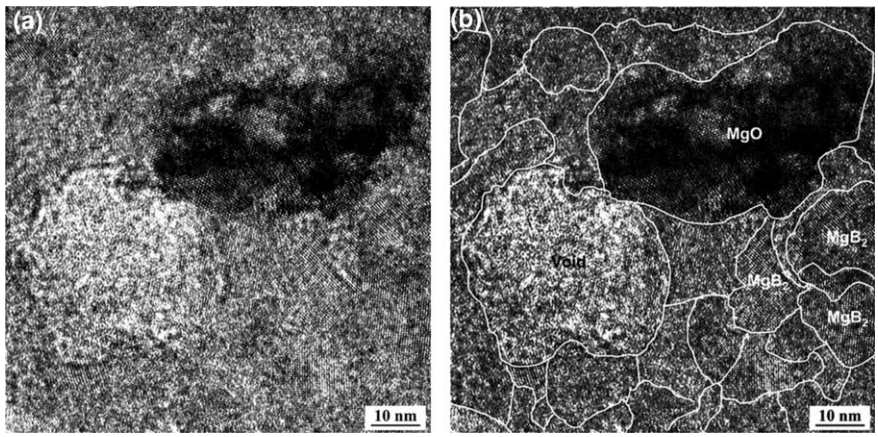

Fig. 3. Cross-sectional high resolution images of the deposited MgB_2 film of specimen A: (a) original image and (b) MgB_2 and MgO grains identified from fast Fourier transformation analysis in the same image.

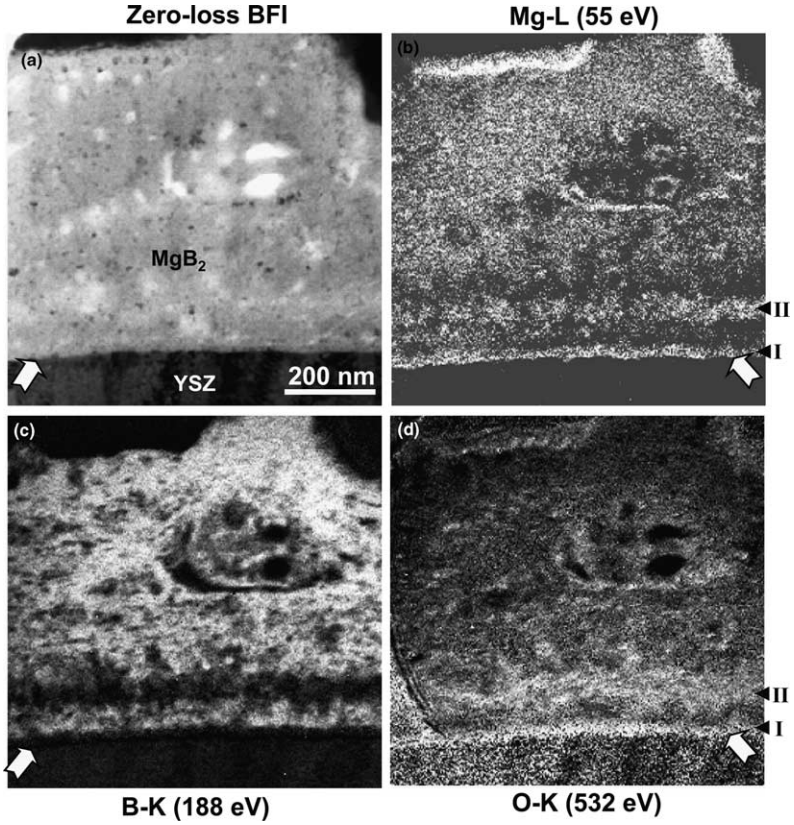

Fig. 4. EELS mapping of specimen A: (a) zero loss bright field image, (b) magnesium, (c) boron, (d) oxygen. Small areas with white contrast both in (b) and (d) are regarded as MgO. The white arrows show the position of the MgB_2/YSZ interface. Regions labeled I and II in (b) and (d) exhibit the magnesium- and oxygen-rich layers, respectively.

distribution between specimen A and specimen B. The layered structure as that shown in Fig. 4 has been also formed near the MgB_2/YSZ interface in specimen B.

4. Discussion

The incorporation of oxygen into the MgB_2 specimens seems to be unavoidable and it may be difficult to determine clearly how the oxygen is incorporated into the MgB_2 specimens. Some possibilities have been assumed [5]: i.e. (1) oxide particles are present in the initial MgB_2 powders, (2) oxide phases are formed during the sintering and (3) the surface oxidation of the MgB_2 at ambient conditions. Generally speaking, all of these assumptions are based on the high solubility of oxygen in magnesium [6,7], and a strong reactivity of the MgB_2 specimen with oxygen at ambient temperature to form $Mg(B,O)_2$ and MgO [8–10].

In the precursor MgB_2/YSZ/Hastelloy film before annealing [11], MgB_2 was inhomogeneously distributed within the amorphous layer on the YSZ/Hastelloy substrate. It was found that MgO and small amounts of voids are also present. These facts suggest that oxygen was possibly incorporated by the causes (1) and (3) described above.

The formation of the layered structure in the films can be interpreted as follows: If oxygen presents in the deposited MgB_2 film during the deposition, magnesium would be firstly oxidized into MgO during the subsequent annealing because of the lower oxygen potential of magnesium than that of boron. The oxygen potential of

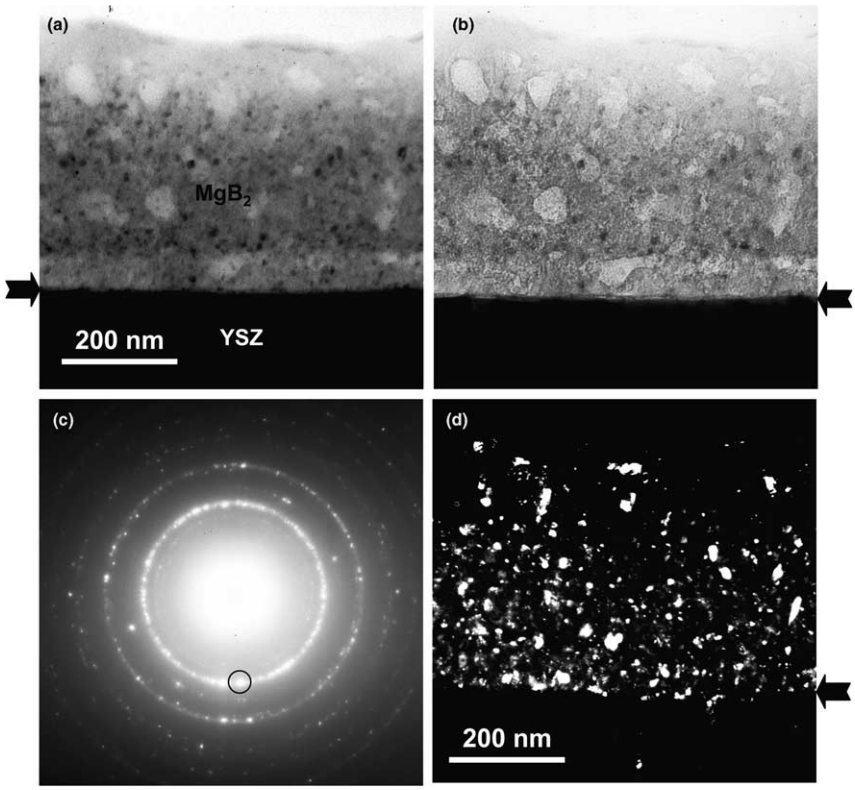

Fig. 5. Cross-sectional TEM image of specimen B: (a) bright field image, (b) under-focused BFI, (c) electron diffraction pattern obtained from the MgB_2 film and (d) dark field image taken with a part of the diffraction ring shown by a small circle in (c). Arrows show the position of the MgB_2/YSZ interface.

magnesium (ΔG) is about -290 kcal/kg mol O_2, which is a little lower than that of boron ($\Delta G \sim -190$ kcal/kg mol O_2) [12]. In the present heat treatments, heating up was conducted from the substrate toward the MgB_2 thin film. Accordingly, there is also a chance that oxygen diffuses from the YSZ buffer layer into the MgB_2 film. Oxidation of the MgB_2 film, therefore, would be initiated at the MgB_2/YSZ interface, resulting into the formation of magnesium- and oxygen-rich layer, while boron was enriched above the magnesium- and oxygen-rich layer. These reactions then formed the layered structure.

As mentioned above, specimen A has a higher value for J_c than specimen B although their microstructural appearances are very similar to each other except the sizes of MgB_2 and MgO grains and voids. There are two probable mechanisms to explain the difference in J_c: (i) The grain boundaries may act as pinning centers [2]. The grain size of specimen A is smaller than that of specimen B. Hence, the interspacing between pinning centers is smaller in specimen A giving higher J_c than specimen B. (ii) Nanostructures that cannot be observed clearly with TEM are present as pinning centers. By annealing at a low temperature (as in specimen A), small MgB_2 grains are formed associated with $Mg(B,O)_2$. The grains of MgB_2 are very small in size and large in number, and they have a good mutual contact with one another. This can give a high electrical conductivity of the specimens that contain an insulating phase such as MgO. At a low temperature, oxygen atoms cannot diffuse well and some domains of MgB_2 still contain a significant amount of oxygen to be $Mg(B,O)_2$ where the concentration of oxygen is plausibly fluctuated. The regions of a high concentration of oxygen have a low critical

temperature [13,14], and they tend to become easily non-superconducting under a high magnetic field. Actually, the critical temperature of specimen A is a little lower than that of specimen B. Then the regions of high oxygen concentration inside $Mg(B,O)_2$ grains, as well as fine grains of MgO, can act as pinning centers. This results in high performance of superconductivity under a high magnetic field. After annealing at a high temperature (as in specimen B), oxygen atoms in $Mg(B,O)_2$ diffuse well to precipitate grains of MgO, leaving grains of almost pure MgB_2. Grains of MgB_2 and MgO have grown large as shown in Fig. 5. There are no $Mg(B,O)_2$ type pinning centers any more in specimen B, resulting in a low value for J_c under a high magnetic field.

5. Conclusions

The TEM study on the two MgB_2 thin films with the different conditions of the heat treatments suggested some important points for fabricating the high performance MgB_2 superconducting films. The fine grain sizes of MgB_2 and MgO (5–30 nm), a good mutual contact of the grains and the small sizes of voids (10–60 nm) were observed in specimen A which was annealed at 873 K. These structural properties provide a higher J_c value of specimen A compared with that of specimen B annealed at 953 K. The result suggests that the nanosized MgO grains, MgB_2 grains containing high concentration of oxygen and grain boundaries may be acting as pinning centers. The elemental analyses revealed that the ''layered structure'', which is characterized as the B-enriched layer sandwiched between the Mg- and O-enriched layers, is formed near the MgB_2/YSZ interface during annealing.

Acknowledgements

This work was supported in part by Nanotechnology Support Project of the Ministry of Education, Culture, Sport, Science and Technology, Japan.

References

[1] J. Nagamatsu, N. Nakagawa, T. Muranaka, Y. Zenitani, J. Akimitsu, Nature 410 (2001) 43.
[2] K. Komori, K. Kawagishi, Y. Takano, H. Fujii, S. Arisawa, H. Kumakura, Appl. Phys. Lett. 81 (2002) 1047.
[3] R. Flukiger, H.L. Suo, N. Musolino, C. Beneduce, P. Toulemonde, P. Lezza, Physica C 385 (2003) 286.
[4] C.F. Liu, G. Yan, S.J. Du, W. Xi, Y. Feng, P.X. Zhang, X.Z. Wu, L. Zhou, Physica C 386 (2003) 603.
[5] D. Eyidi, O. Eibl, T. Wenzel, K.G. Nickel, M. Giovannini, A. Saccone, Micron 34 (2003) 85.
[6] Y. Yan, M.M. Al-Jassim, Phys. Rev. B 67 (2003) 212503-1.
[7] T. Wenzel, K.G. Nickel, J. Glaser, H.J. Meyer, D. Eyidi, O. Eibl, Phys. Status Solidi 2 (2003) 374.
[8] X.Z. Liao, A.C. Serquis, Y.T. Zhu, J.Y. Huang, D.E. Peterson, F.M. Mueller, Appl. Phys. Lett. 80 (2002) 4398.
[9] X.Z. Liao, A.C. Serquis, Y.T. Zhu, J.Y. Huang, L. Civale, D.E. Peterson, F.M. Mueller, Appl. Phys. Lett. 93 (2003) 6208.
[10] R.F. Klie, J.C. Idrobo, N.D. Browning, Appl. Phys. Lett. 80 (2002) 3970.
[11] H. Sosiati et al., unpublished data.
[12] J.F. Elliott, M. Gleiser, Thermochem. Steelmaking I (1960).
[13] S. Patnaik, L.D. Cooley, A. Gurevich, A.A. Polyanskii, J. Jing, X.Y. Cai, A.A. Squitieri, M.T. Naus, M.K. Lee, J.H. Choi, L. Belenky, S.D. Bu, Supercond. Sci. Technol. 14 (2001) 315.
[14] C.B. Eom, M.K. Lee, J.H. Choi, L.J. Belenky, X. Song, L.D. Cooley, M.T. Naus, S. Patnaik, J. Jiang, M. Rikel, A. Polyanskii, A. Gurevich, X.Y. Cai, S.D. Bu, S.E. Babcock, E.E. Hellstrom, D.C. Larbalestier, N. Rogado, K.A. Regan, M.A. Hayward, T. He, J.S. Slusky, K. Inumaru, M.K. Haas, R.J. Cava, Nature 411 (2001) 558.